Insights into the molecular mechanism for hyperpolarization-dependent activation of HCN channels

Galen E. Flynn[a,1] and William N. Zagotta[a]

[a]Department of Physiology and Biophysics, University of Washington, Seattle, WA 98195

Edited by Richard W. Aldrich, The University of Texas at Austin, Austin, TX, and approved July 10, 2018 (received for review March 30, 2018)

Hyperpolarization-activated, cyclic nucleotide-gated (HCN) ion channels are both voltage- and ligand-activated membrane proteins that contribute to electrical excitability and pace-making activity in cardiac and neuronal cells. These channels are members of the voltage-gated Kv channel superfamily and cyclic nucleotide-binding domain subfamily of ion channels. HCN channels have a unique feature that distinguishes them from other voltage-gated channels: the HCN channel pore opens in response to hyperpolarizing voltages instead of depolarizing voltages. In the canonical model of electromechanical coupling, based on Kv channels, a change in membrane voltage activates the voltage-sensing domains (VSD) and the activation energy passes to the pore domain (PD) through a covalent linker that connects the VSD to the PD. In this investigation, the covalent linkage between the VSD and PD, the S4-S5 linker, and nearby regions of spHCN channels were mutated to determine the functional role each plays in hyperpolarization-dependent activation. The results show that: (*i*) the S4-S5 linker is not required for hyperpolarization-dependent activation or ligand-dependent gating; (*ii*) the S4 C-terminal region ($S4_{C\text{-}term}$) is not necessary for ligand-dependent gating but is required for hyperpolarization-dependent activation and acts like an autoinhibitory domain on the PD; (*iii*) the $S5_{N\text{-}term}$ region is involved in VSD–PD coupling and holding the pore closed; and (*iv*) spHCN channels have two voltage-dependent processes, a hyperpolarization-dependent activation and a depolarization-dependent recovery from inactivation. These results are inconsistent with the canonical model of VSD–PD coupling in Kv channels and elucidate the mechanism for hyperpolarization-dependent activation of HCN channels.

SpIH | patch-clamp | voltage-dependent gating | cyclic nucleotide-gated | allostery

Hyperpolarization-activated, cyclic nucleotide-gated (HCN) ion channels are integral membrane proteins that play a crucial role in regulating the membrane excitability of cardiac and neuronal cells (1, 2). HCN channels are members of the voltage-gated Kv channel superfamily, but they have key specializations that make them unique (Fig. 1) (3–6): (*i*) HCN channels are weakly selective for potassium compared with other voltage-gated Kv channels, (*ii*) HCN channels are activated by the direct binding of cyclic nucleotides, and (*iii*) HCN channels are activated by membrane hyperpolarization in contrast to most other voltage-gated Kv channels, which are activated by membrane depolarization (7, 8). The hyperpolarization-dependent activation of HCN channels is critical for their physiological function; however, the underlying mechanism is still unknown (2).

Recently, two cryoelectron microscopy (cryo-EM) structures of the human HCN1 channel (hHCN1) were determined: one in the absence and one in the presence of cAMP, a physiological ligand of HCN channels (PDB ID codes 5U6O and 5U6P, respectively) (9). These hHCN1 structures revealed that each of the subunits comprising the hHCN1 channel tetramer contributes equally to the formation of a centralized pore that regulates ion flow across the membrane (Fig. 1*A*). Each HCN subunit has distinct structural and functional domains (Fig. 1*B*): a transmembrane voltage-sensing domain (VSD: S1–S4) (Fig. 1*B*, blue), a transmembrane pore-forming domain (PD: S5–S6) (Fig. 1*B*, orange), and a cytosolic C-linker (Fig. 1*B*, purple), and cyclic nucleotide-binding domain (CNBD) (Fig. 1*B*, green). The hHCN1 structures also have several unexpected features. The first is a novel cytosolic HCN domain (HCND) (Fig. 1*B*, red) located in the N-terminal region proximal to the VSD. The second is that the transmembrane domains are arranged so the VSDs and PDs are not shared or swapped with other subunits (Fig. 1*A*). This arrangement of transmembrane domains differs from that of most Kv channels, such as Kv1.2-2.1 (PDB ID code 2R9R) (10, 11), but is similar to the structures of other ion channels in the CNBD channel family (e.g., LliK, EAG, hERG, Tax4) (9, 12–16). Finally, the third unexpected feature of the hHCN1 channel is an unusually long S4 helix compared with other voltage-gated channels. The functional role of each of these features is not completely known.

Opening a voltage-gated ion channel pore requires three processes: (*i*) activation of the VSD, (*ii*) propagation of the activation energy from the VSD to the PD, and (*iii*) structural rearrangements in the PD that opens a pore gate for ions to flow across the membrane. In all voltage-gated ion channels, including HCN channels, the positively charged S4 helix in the VSD acts as the membrane voltage-sensor and moves outward with membrane depolarization and inward with hyperpolarization (17–19). The VSD is covalently linked to the PD by the S4–S5 linker (Fig. 1*B*). In the canonical model of VSD–PD coupling, based on Kv channels, the activation energy in the S4 of the VSD passes to the S4–S5 linker via the covalent linkage and then from the S4–S5 linker to the PD via a noncovalent interaction between

Significance

Unlike most other voltage-activated ion channels, hyperpolarization-activated, cyclic nucleotide-gated (HCN) channels open in response to hyperpolarizing membrane voltages. The molecular mechanism that is responsible for this unique voltage dependence in HCN channels is unknown. Here, we show that the covalent linkage between the voltage-sensing domain and the pore domain, the S4-S5 linker, is not required for hyperpolarization-dependent activation or ligand-dependent gating, as previously thought. Instead the voltage-sensing domain is inhibitory on the pore domain, and hyperpolarizing voltages relieve this autoinhibition, allowing the pore to open. This model explains the unique hyperpolarization-dependent activation of HCN channels.

Author contributions: G.E.F. designed research; G.E.F. performed research; G.E.F. and W.N.Z. analyzed data; and G.E.F. and W.N.Z. wrote the paper.

The authors declare no conflict of interest.

This article is a PNAS Direct Submission.

[1]To whom correspondence should be addressed. Email: galen@uw.edu.

This article contains supporting information online at www.pnas.org/lookup/suppl/doi:10.1073/pnas.1805596115/-/DCSupplemental.

Published online August 3, 2018.

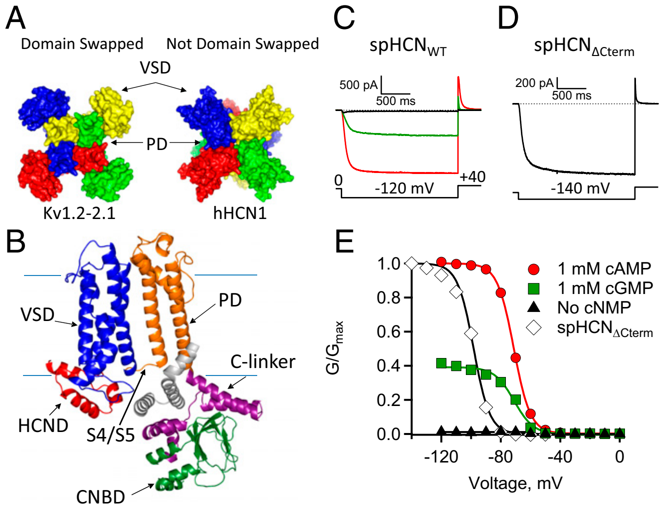

Fig. 1. HCN channels: structure and function. (*A*) Top view of Kv1.2-2.1 (PDB ID code 2R9R) and hHCN1 (PDB ID code 5U6O) with subunits in different colors. (*B*) A subunit of spHCN homology model labeled with VSD (blue), PD (orange), C-linker (purple), CNBD (green), and HCND (red). Also shown is part of the neighboring subunit (gray). (*C* and *D*) ZD7288-subtracted currents measured in the absence of ligand (black, triangles), 1 mM cGMP (green, squares), or 1 mM cAMP (red, circles) (*Materials and Methods*). (*C*) $\mathrm{spHCN_{WT}}$ currents (*D*) $\mathrm{SpHCN_{\Delta Cterm}}$ currents (diamonds). (*E*) *GV* curves with smooth lines that represent Boltzmann fits (*SI Appendix*, Table S1).

the S4–S5 linker and the S6 to open the pore gate (10, 11, 20–24). However, HCN channels are opened by hyperpolarizing voltage steps. It is thought that hyperpolarization-dependent activation in HCN channels results from a reversed VSD–PD coupling where the hyperpolarized state of the VSD is coupled to pore opening (18, 25).

The goal of this investigation was to elucidate the molecular mechanism underlying hyperpolarization-dependent activation in HCN channels. Site-directed mutagenesis techniques were used to mutate the S4–S5 linker and nearby regions of the spHCN channel to determine the functional role each played in hyperpolarization-dependent activation. Surprisingly, the S4–S5 linker was not required for VSD–PD coupling. Instead, VSD–PD coupling required the S4 C-terminal ($\mathrm{S4_{C\text{-}term}}$) and the S5 N-terminal regions ($\mathrm{S5_{N\text{-}term}}$). We propose the $\mathrm{S4_{C\text{-}term}}$ region, along with the $\mathrm{S5_{N\text{-}term}}$ region, acts to inhibit opening of the PD and hyperpolarizing voltages relieve this autoinhibition. The $\mathrm{S5_{N\text{-}term}}$ region also helps hold the pore closed. Together, these results define a model for the mechanism underlying hyperpolarization-dependent activation of HCN channels.

Results

Like other HCN channels, the sea urchin HCN channel ($\mathrm{spHCN_{WT}}$) is hyperpolarization-activated and ligand-gated (26, 27). Recently, cryo-EM structures were solved of the hHCN1 channel in a closed state (9). Interestingly, the hHCN1 S4 helix is longer than the S4 helices of other voltage-gated channel structures. It was previously proposed that an interaction between the C-terminal end of the S4 and the C-linker has a role in hyperpolarization-dependent activation of HCN channels (9, 25, 28, 29). However, the S4 interacting residues in hHCN1, HMTY, are not present in $\mathrm{spHCN_{WT}}$ channels (*SI Appendix*, Fig. S1). Despite missing the HMTY sequence, $\mathrm{spHCN_{WT}}$ channels are opened with hyperpolarizing voltages and binding of ligand, indicating that these residues are not required for hyperpolarization-dependent activation or cyclic nucleotide-dependent gating. Therefore, a structural homology model for spHCN channels was generated based on the hHCN1 structure (PDB ID code 5U6O), but it is missing the four amino acids (HMTY) at the C terminus of the S4 (Fig. 1*B*) (30). With the HMTY sequence missing, the $\mathrm{spHCN_{WT}}$ homology model simply assumes that the S4 helix ends after the sequence QWEQAF where four of these six residues are identical between hHCN1 and $\mathrm{spHCN_{WT}}$. The $\mathrm{spHCN_{WT}}$ homology model was used in this study to structurally represent the location of different mutations.

$\mathrm{SpHCN_{WT}}$ channels expressed robustly in *Xenopus* oocytes. Under symmetrical ionic conditions (*Materials and Methods*), macroscopic $\mathrm{spHCN_{WT}}$ currents, recorded from excised inside-out patches, were elicited from a holding potential of 0 mV to more hyperpolarizing voltages using 2-s test pulses typically in the range of 0 to −140 mV (Fig. 1*C* and *SI Appendix*, Fig. S2). At the end of each experiment, 100 μM ZD7288, a specific HCN channel blocker, was applied to subtract off leak and non-HCN channel currents (*SI Appendix*, Fig. S2 *E* and *F*). As previously shown, $\mathrm{spHCN_{WT}}$ channels were activated by membrane hyperpolarization, not depolarization (26, 27). In response to hyperpolarizing steps and in the absence of ligand, $\mathrm{spHCN_{WT}}$ channels rapidly activated and inactivated, producing only a small transient current (Fig. 1*C*, black trace). However, in the presence of the partial agonist cGMP (1 mM) or the full agonist cAMP (1 mM, saturating concentration), $\mathrm{spHCN_{WT}}$ channels rapidly activated but did not inactivate (Fig. 1*C*, green and red traces, respectively). Instantaneous, leak-subtracted tail currents were measured at the +40-mV tail pulse voltage, then normalized to the maximum currents measured in the presence of 1 mM cAMP (Fig. 1*C* and *SI Appendix*, Fig. S2). Conductance–voltage relationships (*GV* curves) were plotted from these normalized tail currents as a function of test pulse voltage and the *GV* data were fit with the Boltzmann function (Fig. 1*E* and *SI Appendix*, Table S1). The half-activation voltages ($V_{1/2}$), slopes (*s*), and fractional activation of the partial agonist cGMP relative to the full agonist cAMP ($G_{\mathrm{cGMP}}/G_{\mathrm{max,cAMP}}$) were consistent with those previously reported for $\mathrm{spHCN_{WT}}$ channels (*SI Appendix*, Table S1) (31, 32).

SpHCN channels with the C terminus deleted, $\mathrm{spHCN_{\Delta Cterm}}$, still exhibit hyperpolarization-dependent activation but do not inactivate (Fig. 1*D*) (17, 33). In addition, there is a hyperpolarizing shift in voltage dependence of $\mathrm{spHCN_{\Delta Cterm}}$ channels not observed in $\mathrm{mHCN1_{\Delta Cterm}}$ or $\mathrm{mHCN2_{\Delta CNBD}}$ channels (Fig. 1*E*) (17, 33, 34). The lack of inactivation is consistent with previous reports that the C-terminal region of spHCN channels produces inactivation in the absence of cyclic nucleotide, which is relieved by the binding of ligand (17). From these and previously reported results, it is clear that the spHCN C-terminal region is required for ligand-dependent gating but not hyperpolarization-dependent activation.

Modular Gating Scheme for Interpretation of Mutant Effects. To interpret complex changes in the *GV* relationships resulting from our mutations, a modular gating scheme was adopted for the hyperpolarization-dependent activation of spHCN channels using a model developed by Horrigan and Aldrich (HA model) (35) for BK channels (Fig. 2 and *SI Appendix*, Fig. S5). The HA model assumes that the opening conformational change in the PD is allosterically coupled to conformational changes in the VSD and CNBD (Fig. 2*A*). For example, the allosteric coupling between the VSD and the PD means that activation of each VSD causes an *F*-fold change in the closed-to-open equilibrium constant of the PD, and conversely opening of the pore causes an *F*-fold change in the resting-to-activated equilibrium constant of each VSD. In the context of the HA model, an increase in just the equilibrium constant for VSD rearrangement, *H*, produces a simple depolarizing shift in the voltage dependence of activation, with no change in fractional activation by cGMP (Fig. 2*B*). However, an increase in the equilibrium constant of pore opening, *L*, produces a large increase in the fractional activation by cGMP. Finally, a decrease in the VSD–PD coupling, *F*, causes primarily an increase in the steady-state conductance at depolarized voltages where $\mathrm{spHCN_{WT}}$ channels are normally closed. Simultaneous fitting of the HA model to steady-state *GV* curves measured from $\mathrm{spHCN_{WT}}$ channels in 1 mM cAMP and cGMP provided a method to discriminate the mutational effects on the

PHYSIOLOGY

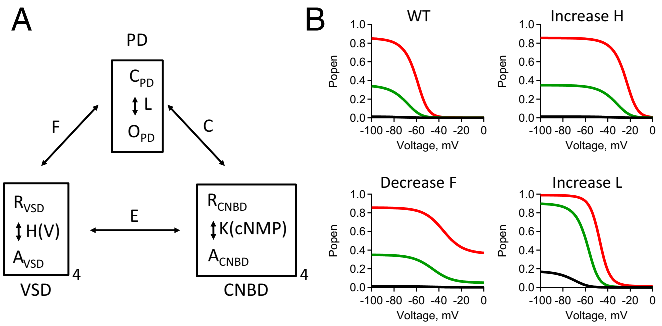

Fig. 2. The HA modular gating scheme used to describe hyperpolarization-dependent activation. (*A*) Schematic of the HA model showing each functional domain PD, VSD, and CNBD (*Materials and Methods*). The equilibrium constants are *L*, *H(V)*, and *K*. The coupling factors are *C*, *F*, and *E*. (*B*) Popen vs. voltage predictions of the HA model for $spHCN_{WT}$ channels. Also shown are predictions when VSD equilibrium constant *H(V)* is increased, the VSD–PD coupling factor *F* is decreased, or the PD equilibrium constant *L* is increased (WT: $H_0 = 0.024$, $V_H = -9.63$ mV, $F = 10.1$, $L = 5.91$, $\alpha\_cAMP = 1$, $\alpha\_cGMP = 0.091$, $\alpha\_NocNMP = 0.0021$; Increase *H*: $H_0 = 1$; decrease $F = 1.8$; increase $L = 100$).

energetics of pore opening, VSD rearrangements, and VSD–PD coupling. While 1 mM cGMP was not fully saturating for most of the spHCN constructs (e.g., for $spHCN_{WT}$ $G_{1mM\_cGMP}/G_{sat\_cGMP} = 0.75$), it was sufficient to assess the free energy change of pore opening of the channels in these experiments (32). Many of the mutant spHCN channels exhibited an increase in steady-state conductance at depolarized potentials. To explain this behavior, the HA model was parameterized, assuming that the resting state of the VSD was autoinhibitory on the PD, inhibiting pore opening by a factor *F*, and the activated (i.e., hyperpolarized) state of the VSD removes this inhibition (*Materials and Methods* and Eqs. **3** and **5**).

The HA model provides adequate fits of the *GV* curves across a broad spectrum of mutational effects by changing only four parameters: H_0 (the equilibrium constant for activation of the VSD at 0 mV with an open pore), V_H (the slope-factor that describes the voltage-dependent rearrangement of the VSD), *L* (the equilibrium constant of pore opening with an activated VSD and cAMP-bound CNBD), and *F* (the coupling coefficient between the VSD and the PD). The HA model was used to quantitatively validate our conclusions using just a few simplifying and explicit assumptions. While the model is oversimplified, it provides a context for interpreting complex changes in the *GV* curves produced by the mutations.

The HA model does not account for spHCN inactivation. Inactivation is unique to spHCN channels and not readily observed in other HCN channels (27). SpHCN inactivation is rapid and thought to occur primarily from preopen closed states (36). As a consequence of inactivation, $spHCN_{WT}$ channels, in the absence of ligand, produce only small transient currents (Fig. 1 *C* and *E*). Because inactivation is poorly understood, it was not included in the HA model. Therefore, in these experiments, the HA model was fit only to the *GV* curves measured from channels in the presence of cAMP or cGMP.

The S4–S5 Linker Is Not Required for Hyperpolarization-Dependent Activation or Ligand-Dependent Gating. The VSD and the PD are connected by the S4–S5 linker, which, in the canonical model of voltage-dependent coupling, acts as the molecular conduit underlying electromechanical coupling between these two domains (Fig. 1*B*) (10, 11, 20–24). This model supposes that movement of each S4 pulls on the S4–S5 linker, which in turn opens a single gate in the pore. Recently, it was demonstrated that split rEAG or hERG channels with a break in the S4–S5 linker are still activated by depolarizing pulses, indicating that the S4–S5 linker is not required for depolarization-dependent activation in these channels (37).

To investigate the functional role of the S4–S5 linker in hyperpolarization-dependent activation of spHCN channels, split channels were made where the S4–S5 linker was broken or completely eliminated. Split spHCN channels were produced when the 767 amino acids of $spHCN_{WT}$ were coexpressed as two separate polypeptides: a VSD-containing polypeptide (#1–359) and a PD-containing polypeptide (#360–767) (*Materials and Methods*) (Fig. 3). The $spHCN_{(359:360)}$ channels, resulting from coexpression of the VSD and PD polypeptides, had a break in the covalent linkage between the S4 helix and the S4–S5 linker. The $spHCN_{(359:363)}$ channels, resulting from the coexpression of the VSD polypeptide and a "truncated" PD polypeptide (#363–767), had the entire S4–S5 linker removed. Amazingly, both $spHCN_{(359:360)}$ and $spHCN_{(359:363)}$ channels were functional and exhibited hyperpolarization-dependent activation and ligand-dependent gating (Fig. 3 *C* and *D* and *SI Appendix*, Table S1). $SpHCN_{(359:363)}$ channels exhibited nearly WT-like hyperpolarization-dependent activation despite missing the entire S4–S5 linker (Fig. 3*D*). Interestingly, $spHCN_{(359:360)}$ channels, with a broken S4–S5 linker, exhibited a small steady-state conductance at depolarizing voltages where $spHCN_{WT}$ channels were normally closed (Fig. 3 *B* and *C*). This steady-state conductance in $spHCN_{(359:360)}$ channels was not due to incomplete assembly of the VSD and PD polypeptides because a fourfold increase in VSD cRNA did not significantly change the relative conductance at depolarized voltages (*SI Appendix*, Fig. S3 *A* and *C* and Table S1). These results indicate that the covalent linkage between the S4 and S5, the S4–S5 linker, is not required for hyperpolarization-dependent activation or ligand-dependent gating.

To mechanistically interpret the mutational effects observed in spHCN channels with a broken S4–S5 linker, the cGMP and cAMP *GV* curves were fit with the HA model (Fig. 3, dashed lines). These split channels did not exhibit a large change in the fractional activation by cGMP ($G_{cGMP}/G_{max,cAMP}$) at hyperpolarizing voltages, suggesting that the mutations had little or no effect on pore opening, *L* (Fig. 2). In the context of the model, the primary effect was a 4.2-fold decrease in *F* for $spHCN_{(359:360)}$ channels with the broken S4–S5 linker compared with $spHCN_{WT}$ channels (Fig. 3 *B* and *C* and Table 1). The finding that the steady-state conductance at depolarized voltages in $spHCN_{(359:360)}$ channels could be explained primarily by a decrease in VSD–PD

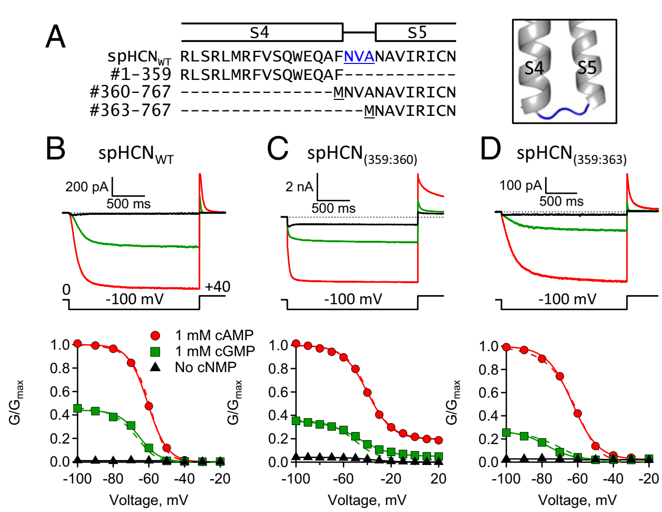

Fig. 3. The S4–S5 linker is not required for hyperpolarization-dependent activation or ligand-dependent gating. (*A*) Sequence alignment and homology model showing the S4 through S5 regions (#344–370) of $spHCN_{WT}$ along with sequences defining split channels. Highlighted in blue are the S4–S5 linker residues. (*B*–*D*) ZD7288-subtracted currents and *GV* curves: (*B*) $spHCN_{WT}$, (*C*) split $spHCN_{(359:360)}$, and (*D*) split $spHCN_{(359:363)}$. Fits of the Boltzmann equation (smooth lines) (*SI Appendix*, Table S1) and the HA model (dashed lines) (Table 1).

coupling, suggested that the intrinsic state preference of the pore was biased toward opening and that the depolarized state of the VSD acts to autoinhibit the PD. In contrast, $spHCN_{(359:363)}$ channels, with a deleted S4–S5 linker, were fit well with F constrained to the value for $spHCN_{WT}$. The difference between the effects of breaking the S4–S5 linker and deleting the S4–S5 linker might be explained by steric hindrance of the untethered S4–S5 linker attached to the PD in $spHCN_{(359:360)}$ channels. From these results, it is clear that the S4–S5 linker is not required for hyperpolarization-dependent activation or ligand-dependent gating in spHCN channels.

The S4 C-Terminal Region Is an Autoinhibitory Domain. If the S4–S5 linker is not required for hyperpolarization-dependent activation of spHCN channels, then what is? The split channel strategy was used to explore the role of the C-terminal region of the S4 helix ($S4_{C\text{-}term}$: #350–359) of spHCN channels. For these experiments, VSD polypeptides were truncated at either $S4_{C\text{-}term}$ residue #355 (ΔEQAF) or #350 (ΔFVSQWEQAF) and then each was coexpressed with the PD polypeptide (#360–767) (Fig. 4). Both $spHCN_{(355:360)}$ and $spHCN_{(350:360)}$ split channels were functional and exhibited ligand-dependent gating with a fractional activation by cGMP similar to $spHCN_{WT}$ channels (Fig. 4 *C* and *D*). In contrast, however, both of these channels exhibited a complete loss of hyperpolarization-dependent activation. The steady-state conductance for these mutant channels did not change much over a voltage range of –100 to +100 mV. As a consequence of these mutations, $spHCN_{(355:360)}$ and $spHCN_{(350:360)}$ split channels resembled cyclic nucleotide-gated (CNG) channels. CNG channels are voltage-independent, ligand-gated ion channels in the CNBD channel family (16, 38, 39). These results show that the $S4_{C\text{-}term}$ region of spHCN channels is important for hyperpolarization-dependent activation but not ligand-dependent gating.

The loss of hyperpolarization-dependent activation in $spHCN_{(355:360)}$ and $spHCN_{(350:360)}$ channels could occur in a number of ways. In the context of the HA model: (*i*) the PD polypeptides might not coassemble with the VSD polypeptides, (*ii*) the PD might be locked open ($L >> 1$), (*iii*) the VSDs might be locked in the active conformation ($H_0 >> 1$), or (*iv*) the VSD–PD coupling might be lost ($F = 1$). Oocytes injected with only PD polypeptides did not produce spHCN currents, indicating that the PD polypeptides alone were insufficient to yield functional channels (*SI Appendix*, Fig. S3) ($n = 10$). Given that the fractional activation by cGMP for both $spHCN_{(355:360)}$ and $spHCN_{(350:360)}$ channels was not different from $spHCN_{WT}$, changes in L were ruled out because a locked-open pore would display a large increase in fractional activation by cGMP. In addition, other mutations in the same area [e.g., $spHCN_{(359:360)}$ channels], which exhibited an appreciable steady-state conductance at depolarized voltages and were fit unambiguously by the HA model, could only be explained by changes in the VSD–PD coupling (Table 1). Therefore, while we cannot distinguish between the third and fourth possibilities for $spHCN_{(355:360)}$ and $spHCN_{(350:360)}$, it seems clear that mutations in the area of the $S4_{C\text{-}term}$ resulted in a decrease in VSD–PD coupling (see below).

Table 1. Parameters of HA model fits to cGMP and cAMP GV data for split channels

Construct	H_0	*Vh* (mV)	*F*	*L*	*n*
$spHCN_{WT}$	0.024 ± 0.01	−9.63 ± 0.2	10.1*	5.91 ± 0.8	11
359:360	0.043 ± 0.01	−9.49 ± 0.7	2.40 ± 0.1[#]	8.08 ± 3.1	6
359:363	0.078 ± 0.02[†]	−12.2 ± 0.7[†]	10.1*	5.11 ± 1.5	4
355:360			1*	1.76 ± 0.8	3
350:360			1*	2.96 ± 0.3	3
350:363			1*	9.49 ± 2.1	5
350:367			1*	82.6 ± 5.8[†]	3
359:367	0.003 ± 0.001	−11.3 ± 0.2[†]	1.75 ± 0.1[#]	85.3 ± 19[†]	7

*Constrained.
[†]$P < 0.05$ by one-way ANOVA, [#]$P < 0.05$ by a one-way *t* test.

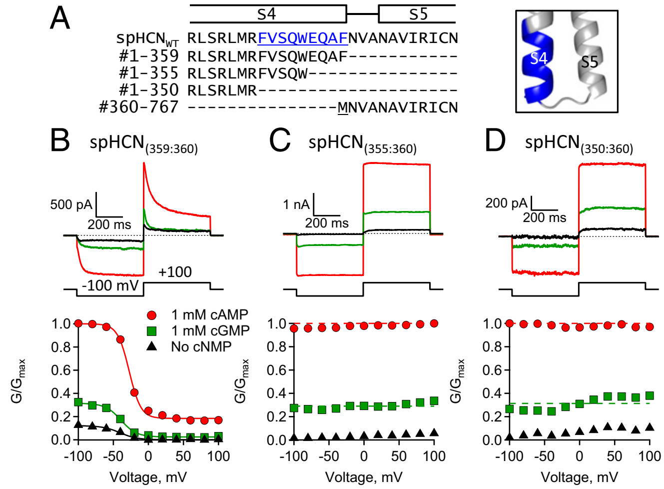

Fig. 4. The $S4_{C\text{-}term}$ region is important for hyperpolarization-dependent activation. (*A*) Sequence alignment and homology model with $S4_{C\text{-}term}$ residues in blue. (*B*–*D*) ZD7288-subtracted currents and *GV* curves: (*B*) split $spHCN_{(359:360)}$, (*C*) split $spHCN_{(355:360)}$, and (*D*) split $spHCN_{(350:360)}$.

Voltage-independent $spHCN_{(355:360)}$ and $spHCN_{(350:360)}$ split channels exhibited ligand-dependent gating with a fractional activation by cGMP that was similar to $spHCN_{WT}$. For the purpose of fitting the HA model to the cGMP and cAMP *GV* data of $spHCN_{(355:360)}$ and $spHCN_{(350:360)}$ split channels, the parameter F was constrained to 1. This removes the coupling between the VSD and PD. An identical fit, however, would be produced if $H_0 >> 1$. Compared with $spHCN_{(359:360)}$ channels (Fig. 4), the HA model fit the *GV* data for $spHCN_{(355:360)}$ and $spHCN_{(350:360)}$ split channels with only a 4.5- and 2.7-fold change in L, respectively. In the context of the model, deleting the spHCN $S4_{C\text{-}term}$ region uncoupled the VSD from the PD and resulted in channels that were only activated by ligand-binding to the CNBD. These results demonstrate that the $S4_{C\text{-}term}$ region is not required for ligand-dependent gating but it is necessary for VSD–PD coupling in spHCN channels.

The $S5_{N\text{-}term}$ Is Important for VSD–PD Coupling and Holding the Pore Closed. In addition to the S4 helix in the VSD, the S4–S5 linker is also covalently linked to the S5 helix of the PD. Is the $S5_{N\text{-}term}$ (#363–367) region involved in hyperpolarization-dependent activation, ligand-dependent gating, or pore opening of spHCN channels? To test for effects on ligand-dependent gating, the $S5_{N\text{-}term}$ region was deleted in split channels with disrupted VSD-PD coupling. In these experiments, two truncated PD polypeptides were each coexpressed with the VSD polypeptide truncated at residue #350 to eliminate VSD–PD coupling (Fig. 5). One PD polypeptide started at residue #363 to remove only the S4–S5 linker [$spHCN_{(350:363)}$] and the other PD polypeptide removed both the S4–S5 linker and the $S5_{N\text{-}term}$ region [$spHCN_{(350:367)}$]. The currents from both $spHCN_{(350:363)}$ and $spHCN_{(350:367)}$ split channels were largely voltage-independent, although some decay was observed with voltage steps from –100 to +100 mV (Fig. 5 *C* and *D*). These mutant channels exhibited ligand-dependent gating; however, the fractional activation by cGMP for $spHCN_{(350:367)}$ channels was substantially larger than $spHCN_{WT}$, $spHCN_{(350:360)}$, or $spHCN_{(350:363)}$ channels (Figs. 3*B* and 5), suggesting that the $S5_{N\text{-}term}$ region is involved in holding the pore closed.

To test for effects on hyperpolarization-dependent activation, the $S5_{N\text{-}term}$ region was deleted in split channels with functional VSD–PD coupling. The full VSD polypeptide (#1–359) was coexpressed with either the PD polypeptide that

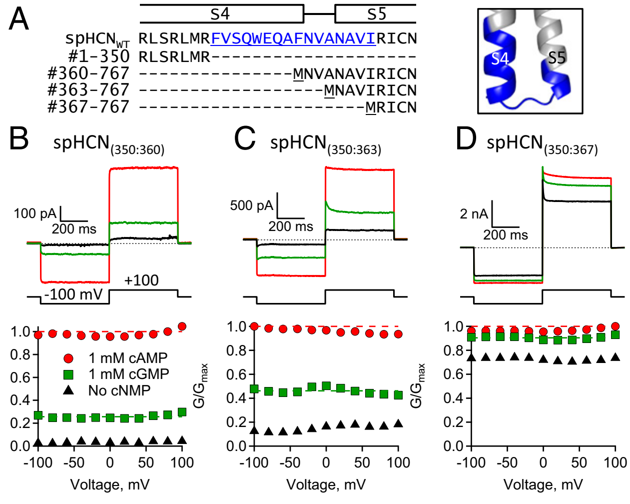

Fig. 5. The $S5_{N\text{-term}}$ region helps keep spHCN channels closed. (*A*) Sequence alignment and homology model with $S4_{C\text{-term}}$ and $S5_{N\text{-term}}$ residues in blue. (*B*–*D*) ZD7288-subtracted currents and *GV* curves: (*B*) split $spHCN_{(350:360)}$, (*C*) split $spHCN_{(350:363)}$, and (*D*) split $spHCN_{(350:367)}$.

removed only the S4–S5 linker [$spHCN_{(359:363)}$] or the PD polypeptide that removed both the S4–S5 linker and the $S5_{N\text{-term}}$ region [$spHCN_{(359:367)}$] (Fig. 6). Both $spHCN_{(359:363)}$ and $spHCN_{(359:367)}$ split channels were functional and exhibited hyperpolarization-dependent activation and ligand-dependent gating. Interestingly, neither exhibited inactivation in the absence of ligand (Fig. 6 *B* and *C*). The *GV* curves of $spHCN_{(359:367)}$ split channels, in which the $S5_{N\text{-term}}$ region was deleted, exhibited a substantial increase in the fractional activation by cGMP and an appreciable conductance at depolarizing voltages where $spHCN_{(359:363)}$ split channels were closed. Like $spHCN_{(359:360)}$ channels, the conductance at depolarized voltages in $spHCN_{(359:367)}$ channels was not due to incomplete assembly of the VSD and PD polypeptides, as a fourfold increase in VSD cRNA did not significantly change the relative conductance at depolarized voltages (*SI Appendix*, Fig. S3 *B* and *D* and Table S1). Together, these results suggest that the $S5_{N\text{-term}}$ region is involved in hyperpolarization-dependent activation as well as holding the pore closed.

To interpret the mutational effects observed when the $S5_{N\text{-term}}$ region was deleted, the *GV* curves were fit with the HA model (dashed lines, Figs. 5 and 6). The main effect of deleting the $S5_{N\text{-term}}$ region in voltage-independent $spHCN_{(350:367)}$ channels was an increase in the fractional activation by cGMP. The HA model fit the data for voltage-independent $spHCN_{(350:367)}$ channels with a greater than 27-fold increase in the equilibrium constant, *L*, compared with $spHCN_{(350:360)}$ channels (Fig. 5 *B* and *D* and Table 1). Similarly, the HA model fit the *GV* curves of voltage-dependent $spHCN_{(359:367)}$ channels with a 16-fold increase in the equilibrium constant, *L*, compared with $spHCN_{(359:363)}$ channels (Fig. 6 *B* and *C*). In addition, there was over a fivefold decrease in *F* for the voltage-dependent $spHCN_{(359:367)}$ channels. Therefore, in the context of the model, the mutational effects of deleting the $S5_{N\text{-term}}$ region were interpreted as a shift in the closed-to-open equilibrium of the PD toward opening and a large decrease in VSD–PD coupling. These results support the conclusion that the $S5_{N\text{-term}}$ region plays a role in both VSD–PD coupling and in holding the pore closed in spHCN channels.

Role of Conserved Residues in $S4_{C\text{-term}}$ Region. When the $S4_{C\text{-term}}$ residues FVSQWEQAF (#351–359) were deleted, $spHCN_{(350:360)}$ split channels were no longer hyperpolarization-activated (Fig. 4*D*). Many of these residues are conserved within the HCN channel family, which has the consensus sequence motif R(Y/F)xxQWExxF (*SI Appendix*, Fig. S1). In addition, the hHCN1 structures reveal that several of these conserved residues form electrostatic interactions with other nearby residues in the resting state (9). To explore the functional role of this motif, two mutant channels were made by substituting alanine for amino acids EQAF (spHCN-A4: #356–359) or F351+QWEQA (spHCN-A6: #351,354-358), respectively, in the full-length polypeptide (#1–767) (Fig. 7). Both spHCN-A4 and spHCN-A6 channels were functional and exhibited hyperpolarization-dependent activation, ligand-dependent gating, and inactivation in the absence of ligand. Interestingly, the *GV* curves measured from these channels in the absence of ligand had a distinctive bell shape (Fig. 7 *C* and *D*). Also, as seen in some of the split channels, spHCN-A4 and spHCN-A6 channels in the presence of cAMP exhibited an appreciable conductance at depolarizing potentials where $spHCN_{WT}$ channels are normally closed. The HA model did not produce adequate fits to the *GV* data of spHCN-A6 channels. However, the HA model did fit the *GV* data of spHCN-A4 channels with a fourfold decrease in *F* compared with $spHCN_{WT}$ channels (Fig. 7*C*, dashed lines, and Table 2). In the context of the model, the primary effect of the alanine mutations in spHCN-A4 channels was a decrease in VSD–PD coupling, which is consistent with our earlier conclusion that deletions of the $S4_{C\text{-term}}$ are associated with a decrease in coupling.

Alanine substitutions were used to explore the role of individual residues in the conserved $S4_{C\text{-term}}$ motif, R(Y/F)xxQWE (Fig. 8). To identify residues in the $S4_{C\text{-term}}$ region of spHCN channels that were important for hyperpolarization-dependent activation, the following individual mutant spHCN channels were made: R350A, F351A, Q354A, W355A, and E356A. Each of these mutant channels was functional and exhibited hyperpolarization-dependent activation, ligand-dependent gating, and inactivation in the absence of ligand (Fig. 8 *B*–*F*). Only spHCN-W355A channels produced currents too small to confirm inactivation in the absence of ligand (Fig. 8*E*). Interestingly, R350A and E356A mutant channels exhibited an appreciable conductance at depolarizing potentials, where $spHCN_{WT}$, F351A, Q354A, and W355A channels were all closed. In addition, the *GV* curves measured from R350A, F351A, and E356A mutant channels in the absence of ligand showed a distinctive bell shape (Fig. 8 *B, C,* and *F*). The arginine

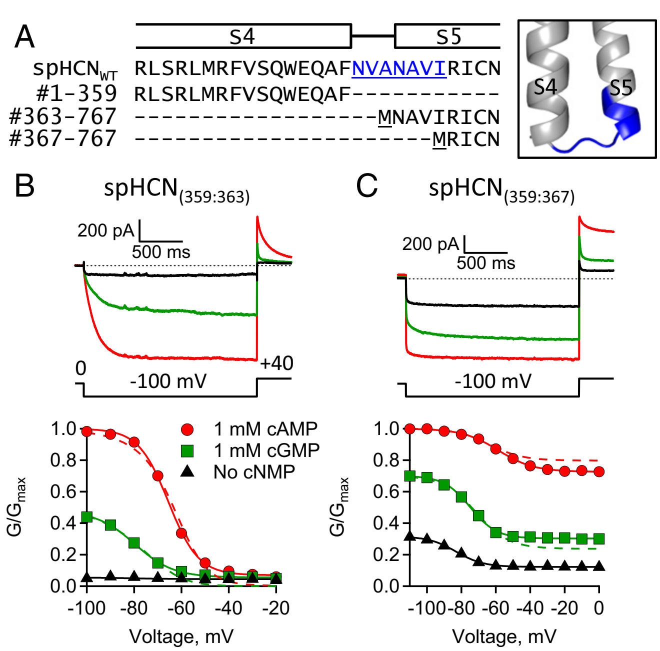

Fig. 6. The $S5_{N\text{-term}}$ region is involved in VSD–PD coupling. (*A*) Sequence alignment and homology model showing S4–S5 linker and $S5_{N\text{-term}}$ residues in blue. (*B* and *C*) ZD7288-subtracted currents and *GV* curves: (*B*) split $spHCN_{(359:363)}$ and (*C*) split $spHCN_{(359:367)}$.

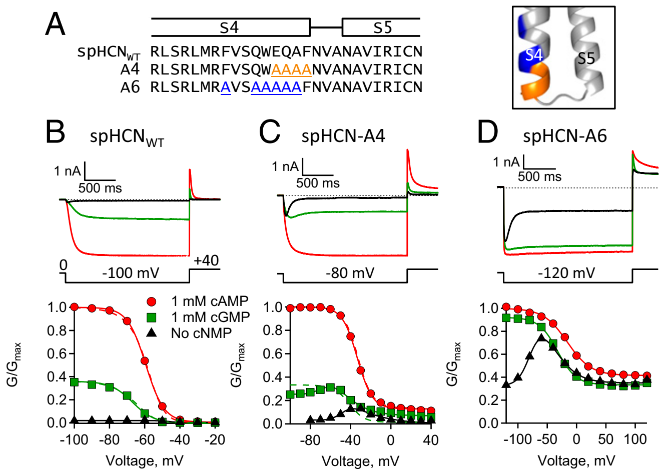

Fig. 7. Mutations in the $S4_{C\text{-term}}$ region reveal two voltage-dependent processes. (*A*) Sequence alignment and homology model with $S4_{C\text{-term}}$ residues highlighted in orange or blue. (*B–D*) ZD7288-subtracted currents and *GV* curves: (*B*) intact spHCN$_{WT}$, (*C*) spHCN-A4, and (*D*) spHCN-A6.

and glutamate residues are conserved between spHCN and hHCN1 and appear to form interactions with residues in nearby transmembrane helices (Fig. 8*A* and *SI Appendix*, Fig. S1) (9). These results suggest that the R350A and E356A mutations perturbed hyperpolarization-dependent activation and that specific interactions in the $S4_{C\text{-term}}$ are important for VSD–PD coupling.

In the context of the model, the primary effects of the R350A and E356A mutations were about a 3.5-fold and 3-fold decrease in *F*, respectively, compared with spHCN$_{WT}$ channels (Table 2). The larger *F* effect observed with the QWE deletions in split channels relative to the individual point mutations of QWE could result from either subthreshold effects of Q354A and W355A, or the fact that the QWE deletion removes the polypeptide backbone in addition to the side chains. An additional effect of the R350A mutation was a greater than 86-fold increase in H_0, the equilibrium constant for the VSD resting-to-activated transition, which accounts for the large depolarizing shift in the *GV* curve (*SI Appendix*, Table S1). The R350 residue is the final positive charge in the spHCN S4 helix and breaking a putative R350:D300 interaction probably contributes to the energetics and voltage dependence of the VSD resting-to-activated transition (Fig. 8*A*). In contrast, fits of the HA model to the F351A and Q354A *GV* curves were similar to spHCN$_{WT}$ channels (Table 2). In the context of the model, R350A caused an increase in the equilibrium constant, H_0, for the VSD resting-to-activated transition, and both R350A and E356A mutations decreased the energetics of VSD–PD coupling. These results support the conclusions that the $S4_{C\text{-term}}$ region exerts an autoinhibitory effect on the PD and that specific interactions involving residues the $S4_{C\text{-term}}$ are important for VSD–PD coupling.

Predicted $S5_{N\text{-term}}$–$S6_{C\text{-term}}$ Salt-Bridge Is Important for Holding the Pore Closed. Previously, Sanguinetti and coworkers (29) demonstrated a salt-bridge interaction in mouse HCN2 channels between an arginine in the $S5_{N\text{-term}}$ and an aspartate in the $S6_{C\text{-term}}$. A homologous interaction is predicted for residues R367 and D471 of spHCN channels (Fig. 8*A*). To test the functional role of this putative interaction in spHCN channels, residues R367 and D471 were individually mutated to alanine. Each of these mutant channels was functional and exhibited hyperpolarization-dependent activation and ligand-dependent gating, but neither inactivated in the absence of ligand (Fig. 8 *G* and *H*). For both mutant channels, however, there was a large increase in the fractional activation by cGMP compared with spHCN$_{WT}$ channels (*SI Appendix*, Table S1). An increase in fractional activation was seen not only in cGMP but also in the absence of ligand. Therefore, it seemed likely that the R367A and D471A mutations were affecting the closed-to-open equilibrium of the PD. For both of these mutants, the fractional activation by cGMP was essentially equal to 1, indicating that *L* must be greater than 500, assuming that we could detect a 2% difference in conductance between cGMP and cAMP at hyperpolarizing voltages (Fig. 8 *G* and *H*, dashed lined, and Table 2). This corresponds to a greater than 85-fold change in *L* relative to spHCNwt. The other parameters for the HA model fits were similar to spHCN$_{WT}$ channels. So, in the context of the model, the R367A and D471A mutations shifted the closed-to-open transition toward opening consistent with the interpretation that an interaction between the $S5_{N\text{-term}}$ and the $S6_{C\text{-term}}$ is important for holding the pore closed.

Inactivation Is Voltage-Dependent. SpHCN channels undergo an inactivation process that is rapid and thought to occur primarily from preopen closed states (*SI Appendix*, Fig. S4*A*). Previously, it was proposed that the mechanism underlying inactivation in spHCN is a reclosure of the activation gate in the form of slippage or desensitization to voltage (36). However, the molecular mechanism for inactivation is still unknown. In spHCN$_{WT}$ channels, inactivation is eliminated by the binding of cyclic nucleotide to the CNBD or the deletion of the C terminus (Fig. 1). In this investigation, one of the striking features of many of the mutant channels measured in the absence of ligand was a bell-shaped *GV* curve, which was due to the combination of activation and inactivation. This was particularly obvious in the mutant channels spHCN-A4 and spHCN-A6 (Fig. 7 *C* and *D*) and spHCN-R350A and spHCN-E356A (Fig. 8 *B* and *F*). These steady-state bell-shaped *GV* curves cannot arise from a voltage-independent inactivation transition that is coupled to hyperpolarization-dependent activation (*SI Appendix*, Fig. S4). They can occur (*i*) if the inactivation transition itself is intrinsically voltage-dependent or (*ii*) if inactivation is coupled to a voltage-dependent transition that is distinct from hyperpolarization-dependent activation. The bell-shaped *GV* curves indicate that there are two separate voltage-dependent processes with opposite voltage dependences that are coupled to channel opening. The right half of the *GV* curve arises from a hyperpolarization-dependent activation of the channel while the left half of the *GV* curve arises from a depolarization-dependent recovery from inactivation. Fitting these *GV* curves with a function equal to the product of two Boltzmann equations reveals an equivalent charge movement for inactivation of ~three electronic charges (*SI Appendix*, Table S1). These results suggest that inactivation in spHCN channels is voltage-dependent.

Can these two voltage-dependent processes be isolated? Yes, hyperpolarization-dependent activation is isolated from inactivation by applying ligand, which removes inactivation (25, 36, 40). To isolate the voltage-dependent inactivation, two mutant channels were studied that did not undergo hyperpolarization-dependent activation: (*i*) spHCN$_{\Delta QWE}$ channels had S4 residues #354–356 deleted from the full-length channel polypeptide and

Table 2. Parameters of HA model fits to GV data for mutant full-length channels

Construct	H_0	*Vh* (mV)	*F*	*L*	*n*
spHCN$_{WT}$	0.024 ± 0.01	−9.63 ± 0.2	10.1*	5.91 ± 0.8	11
A4	0.020 ± 0.009	−7.78 ± 0.5	2.55 ± 0.1$^{\#}$	3.14 ± 0.05	3
R350A	2.07 ± 1.03†	−13.5 ± 1.0†	2.86 ± 0.3$^{\#}$	4.01 ± 1.1	3
F351A	0.008 ± 0.002	−10.5 ± 0.2	10.1*	4.62 ± 0.9	3
Q354A	0.040 ± 0.020	−10.0 ± 1.4	10.1*	2.92 ± 1.0	3
E356A	0.024 ± 0.003†	−11.1 ± 0.3	3.31 ± 0.04$^{\#}$	12.9 ± 3.4†	3
R367A	0.003 ± 0.001	−8.97 ± 0.4	10.1*	>500*	3
D471A	0.006 ± 0.003	−10.0 ± 1.1	10.1*	>500*	3

*Constrained.
$^{\dagger}P < 0.05$ by one-way ANOVA, $^{\#}P < 0.05$ by a one-way *t* test.

PHYSIOLOGY

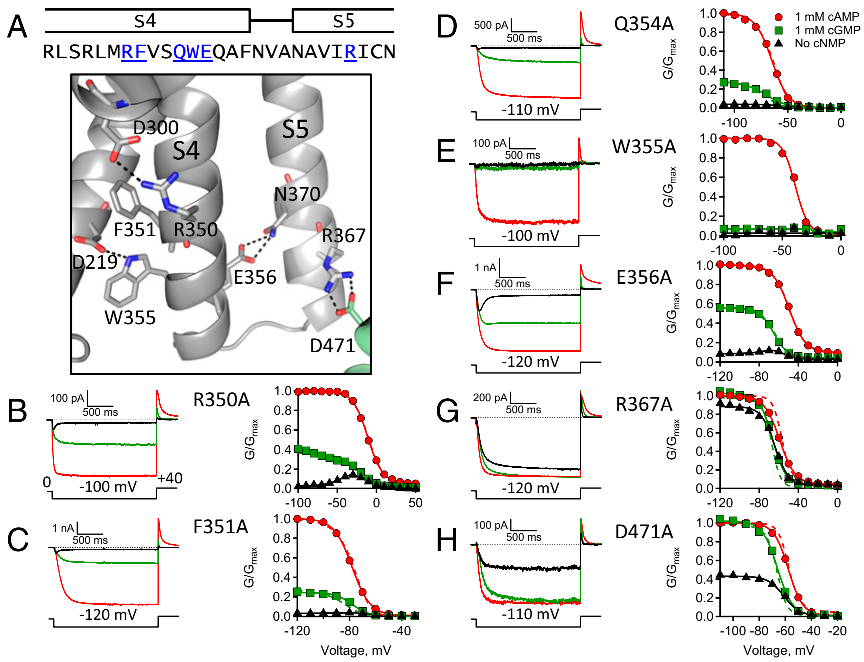

Fig. 8. Functional effects of individual mutations of conserved residues in the $S4_{C\text{-term}}$. (*A*) Sequence alignment with some conserved $S4_{C\text{-term}}$ and $S5_{N\text{-term}}$ residues in blue. The homology model showing residues with side-chains and putative interactions (*A*, *Lower*). (*B*–*H*) ZD7288-subtracted currents and *GV* curves: (*B*) R350A, (*C*) F351A, (*D*) Q354A, (*E*) W355A, (*F*) E356A, (*G*) R367A. Note: these currents were not leak-subtracted with ZD7288. (*H*) D471A.

(*ii*) $spHCN_{\Delta QAF}$ channels had S4 residues #357–359 deleted (Fig. 9). Both mutant channels were functional and exhibited ligand-dependent gating but not hyperpolarization-dependent activation in cAMP. However, both channels exhibited some inactivation with hyperpolarizing pulses in the absence of ligand (Fig. 9 *C* and *D*). The *GV* curves measured from channels in the presence of cAMP were largely voltage-independent in the range of −100 to +100 mV. However, in the absence of ligand, both channels exhibited a voltage-dependent increase in conductance with depolarizing voltage steps. This is particularly evident in the *GV* curve for $spHCN_{\Delta QAF}$, which was fit with a Boltzmann function and suggested an equivalent charge movement of ∼three electronic charges, similar to the charge movement seen for inactivation in mutant channels with bell-shaped *GV* curves. These results suggest that the increase in conductance is due to the depolarization-dependent recovery from inactivation. Therefore, $spHCN_{WT}$ channels have two separate voltage-dependent processes: a hyperpolarization-dependent activation and a depolarization-dependent recovery from inactivation.

Discussion

The goal of this study was to elucidate the mechanism underlying hyperpolarization-dependent activation of HCN channels. Site-directed mutagenesis techniques were used to perturb the S4–S5 linker and nearby regions of the spHCN channel to determine the functional role each played in VSD activation, pore opening, and VSD–PD coupling. The major findings of this investigation are: (*i*) the S4–S5 linker is not required for hyperpolarization-dependent activation or ligand-dependent gating; (*ii*) the $S4_{C\text{-term}}$ region is not necessary for ligand-dependent gating but is required for hyperpolarization-dependent activation and acts like an autoinhibitory domain on the PD; (*iii*) the $S5_{N\text{-term}}$ region is involved in VSD–PD coupling and holding the pore closed; and (*iv*) spHCN channels have two voltage-dependent processes, hyperpolarization-dependent activation and depolarization-dependent recovery from inactivation.

In the canonical model of voltage-dependent coupling, based on depolarization-activated Kv channels (e.g., Shaker and Kv1.2-2.1), the positively charged S4 moves outward in response to depolarizing voltage pulses and in doing so it pulls on the S4–S5 linker, which in turn opens a pore gate (10, 11, 20–24). Recently, however, a noncanonical coupling mechanism was proposed for Kv channels that involves interactions between the S4 and S5 helices (22, 37, 41, 42). Both the movement of the S4 and the location of the pore gate are conserved between hyperpolarization-activated HCN channels and depolarization-activated Kv channels (26, 31, 43–45). In spHCN channels, breaking or deleting the entire S4–S5 linker does not disrupt hyperpolarization-dependent activation or cyclic nucleotide-dependent gating (Fig. 3). Similarly, the S4–S5 linker can be broken and even deleted entirely from depolarization-activated rEAG and hERG channels without disrupting depolarization-dependent activation (37, 41, 42). Therefore, the S4–S5 linker is not required for VSD–PD coupling, hyperpolarization-dependent activation, or ligand-dependent gating of spHCN channels.

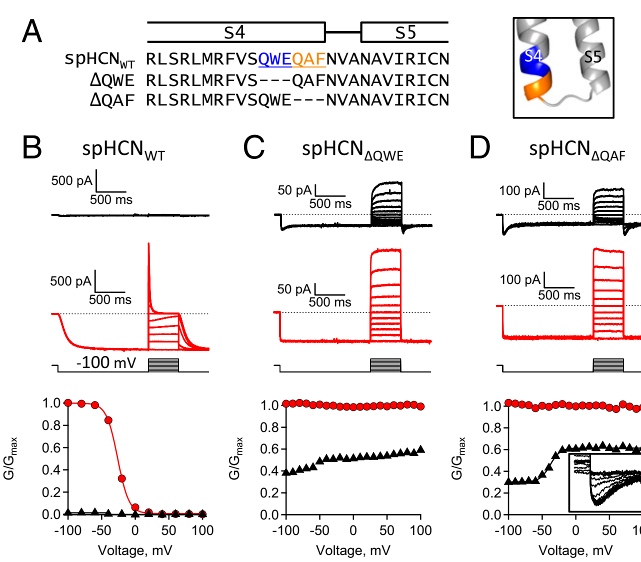

Fig. 9. Deletion of QAF reveals a depolarization-dependent activation. (*A*) Sequence alignment and homology model with $S4_{C\text{-term}}$ residues highlighted in blue or orange. Voltage protocol included a 1.5-s prepulse (−100 mV), 500-ms test pulses (−100 to +100 mV), and tail pulse (−100 mV). (*B*–*D*) ZD7288-subtracted currents and *GV* curves: (*B*) $spHCN_{WT}$, (*C*) $spHCN_{(\Delta QWE)}$, and (*D*) $spHCN_{(\Delta QAF)}$ channels. (*Inset*) Enlargement of tail currents.

The hHCN1 channel structure revealed that the VSD and PD are not shared or swapped between subunits (9). In addition to hHCN1, the VSDs and PDs of other channels in the CNBD subfamily are also not swapped, including a depolarization-activated rEAG channel, a depolarization-activated hERG channel, a voltage-independent (Tax4) channel, and a bacterial CNG channel (LliK) (5, 9, 12, 15, 16, 46). Therefore, the difference between depolarization-dependent activation and hyperpolarization-dependent activation cannot be explained by a lack of domain swapping between subunits of the PDs.

For many depolarization-dependent Kv channels (e.g., Shaker), the intrinsic state preference of the pore is biased toward closing (47). In contrast, the spHCN channel pore prefers being open, a conclusion supported by the many mutations in this study that decreased coupling and resulted in an appreciable steady-state conductance at depolarized voltages. Like spHCN channels, the pore of depolarization-dependent rEAG channels is also biased toward opening (37, 41, 42). Therefore, the difference between depolarization-dependent activation and hyperpolarization-dependent activation cannot be explained by an intrinsic open-state preference of the pore.

Hyperpolarization-dependent activation is a defining property of the entire HCN channel family. What is the mechanism of hyperpolarization-dependent activation in HCN channels? We propose a simple model to explain hyperpolarization-dependent activation in HCN channels (Fig. 10). The movement of the S4 voltage sensor, caused by hyperpolarizing voltage steps, relieves an allosteric inhibitory effect on the PD produced by the VSD, which allows the pore to open. Pore opening is further stabilized by the binding of cAMP to the CNBD. This model can explain the intrinsic open-state dependence of the PD and hyperpolarization-dependent activation in spHCN channels.

Previous work by Yellen and coworkers (28, 31, 40) shows that cross-linking either the $S4_{C\text{-term}}$, the S4–S5 linker, or the $S5_{N\text{-term}}$ to the C-linker region results in spHCN channels that are "locked closed" or "locked open." While the S4–S5 linker is not required for VSD–PD coupling in spHCN channels, cross-linking the S4–S5 linker to the C-linker is likely to trap the VSD or PD of spHCN channels in a resting or activated conformation. In addition, Ryu and Yellen (40), using locked-open and locked-closed mutants of spHCN channels, show that the voltage dependence of gating charge movement (*QV* curves) shifts to either positive voltages for locked-open channels or negative voltages for locked-closed channels (28, 40). Their VSD–PD coupling factors ranged from 3 to 7, somewhat less than the estimates of the VSD–PD coupling factor, *F*, in this study (Tables 1 and 2). For the HA model, a coupling factor of 3–7 would produce significantly more conductance at depolarized voltages than was observed for $spHCN_{WT}$ channels or some of the mutant channels. Overall, however, these results suggest that VSD–PD coupling in spHCN channels is weak compared with *Shaker* and Kv channels, which have coupling factors >100 per voltage sensor (48). Also interesting, Prole and Yellen (25) cross-linked the $S4_{C\text{-term}}$ residue F359C to the C-linker residue K482C and caused spHCN channels to exhibit depolarization-dependent activation. The *GV* curve for the "reversed" gating of these locked-open F359C:K482C channels is similar to $spHCN_{\Delta QAF}$ channels where deletion of $S4_{C\text{-term}}$ residues reveals a depolarization-dependent activation process (Fig. 9*D*). Together, these results support the conclusion that there are two voltage-dependent processes in spHCN channels: a hyperpolarization-dependent activation and a depolarization-dependent recovery from inactivation.

Previously, it was proposed that the mechanism underlying inactivation in spHCN channels is a reclosure of the activation gate in the form of "slippage" or desensitization to voltage (36). This mechanism proposes that movement of the VSD creates a strain on the coupling between the VSD and the PD that can slip before channel opening, resulting in stable closure of the activation gate even at activating voltages. However, our findings that hyperpolarization-dependent activation of spHCN channels involves relief of autoinhibition of the pore by the VSD is incompatible with a slippage mechanism for inactivation. Slippage in a channel with autoinhibition would occur more from the resting closed state and would result in activation (i.e., channel opening) not inactivation. In addition, the finding that inactivation is intrinsically voltage-dependent also suggests that it is moving charge in the membrane electric field, which is also not expected for slippage. For these reasons, it seems likely that inactivation involves a mechanism other than slippage or desensitization to voltage.

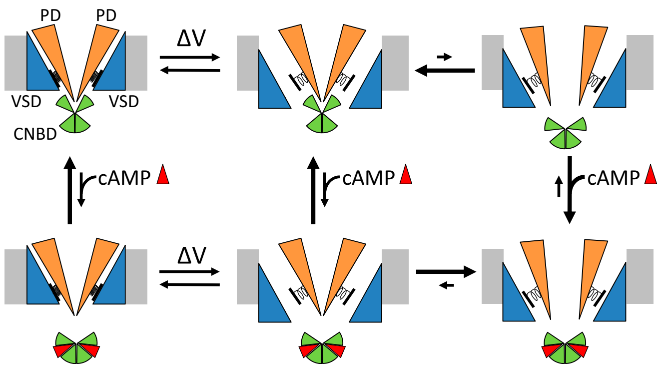

Fig. 10. Model of hyperpolarization-dependent activation for HCN channels. Hyperpolarization causes movement of the VSD (blue) which relieves autoinhibition of the PD (orange). The binding of cyclic nucleotide (red) to the CNBD (green) removes autoinhibition of the PD.

Materials and Methods

Molecular Biology and Channel Expression. The sea urchin HCN channel ($spHCN_{WT}$) cDNA (a gift from U. B. Kaupp, Molecular Sensory Systems, Center of Advanced European Studies and Research, Bonn, Germany; GenBank: Y16880) was subcloned into the high-expression vector plasmid pGEMHE between the 5′ and 3′ Xenopus β-globin gene UTR (27, 49). Site-directed mutagenesis was performed using PCR and confirmed by Sanger DNA sequencing (Genewiz). For protein expression in *Xenopus* oocytes, cRNAs were synthesized by runoff in vitro transcription following the manufacturer's protocol for the HiScribe T7 ARCA mRNA Kit (with tailing) [New England Biolabs; catalog (cat.) #E2060S]. Cyclic nucleotides (cAMP: adenosine-3′,5′-cyclic monophosphate; cat. #A6885 and cGMP: guanosine-3′,5′-cyclic monophosphate; cat. #G6129) were purchased from Sigma-Aldrich. An HCN channel specific pore-blocking compound, ZD7288, was purchased from Tocris (Tocris BioScience; cat. #1000). All other chemicals were purchased through Fisher Scientific.

Split spHCN channels were generated from two separate constructs. One construct, VSD-polypeptide, contained the cDNA sequence encoding all the amino acids from residue 1 to 359 followed by a stop codon. The second construct, PD-polypeptide, started with a methionine codon and contained a cDNA sequence encoding the amino acids starting with residue 360 through to the end of the C terminus (residue 767). For generating split spHCN channels, oocytes were injected with 50 nl of a 1:1 ratio of VSD-encoded cRNA and PD-encoded cRNA. Oocytes were incubated at 16–18 °C until used for patch-clamp recordings experiments.

Homology Model of spHCN. Structures of the hHCN1 channel were recently solved using cryo-EM [(9); pdb:5u6o, 5u6p]. SWISS-MODEL, a web-based protein structure homology-modeling server, used the hHCN1 structures as a template to generate a spHCN homology model based on a protein sequence alignment (spHCN #160-675; hHCN1 #106-620) (30). The structure figures were made using PyMOL software (Schrodinger).

Electrophysiology. All procedures were conducted in accordance with Institutional Care and Use Committee (IACUC)-approved protocols overseen by the Office of Animal Welfare at the University of Washington. *Xenopus* oocytes were harvested and injected with cRNAs as previously described (32, 33). SpHCN currents were recorded using the patch-clamp technique from excised, inside-out patches (50). All recordings were made at room temperature (20–22 °C). Recording electrodes were made from borosilicate glass (Warner Instruments, cat. #G150-4) that was polished to resistances of 0.4–0.8 mΩ. Both the extracellular and intracellular solutions contained (in mM): 130 KCl, 0.2 EDTA, and 3 Hepes at pH 7.2. Cyclic nucleotides, 1 mM cAMP and 1 mM cGMP, were applied to the intracellular surface of patches using a rapid solution changer (RSC-100, Biologic). Typically, HCN currents were isolated by leak subtracting currents recorded in a solution containing 1 mM cAMP and 100 μM ZD7288 at the end of each experiment (*SI Appendix*, Fig. S2 *E* and *F*) (28, 32). Macroscopic currents were low-pass filtered at 2 kHz and digitized at 10 kHz by an EPC10 amplifier (HEKA Instruments Inc.), then analyzed using PatchMaster software (HEKA Instruments Inc.). Data were stored in files for offline analysis using Igor software (Wavemetrics, Inc.) or Excel software (Microsoft Corp.).

Data Analysis. For conductance-voltage relationships (GV curves), the relative conductance was determined by measuring the instantaneous tail currents typically at +40 mV which were then normalized to the maximum conductance measured in 1 mM cAMP. The resulting GV curves were fit with the Boltzmann function in the form:

$$\frac{G}{G_{max,cAMP}} = \left(\frac{1-A}{1+e^{\left(-\left(V-V_{½}\right)/s\right)}}+A\right) \quad [1]$$

where $G/G_{max,cAMP}$ is the relative conductance as a fraction of the maximum conductance in cAMP, V is the membrane voltage, $V_{½}$ is the half-maximal activation voltage, s is the slope representing the steepness of the voltage-dependence, and A is the relative conductance at depolarized voltages. It is noteworthy that spHCN channels were slow to activate and did not always reach steady-state at the end of a 2 sec test pulse voltages, which caused a slight negative shift in $V_{½}$. In some cases, it was necessary to fit the data with an equation equal to the product of two Boltzmann functions in the form:

$$\frac{G}{G_{max,cAMP}} = \left(\frac{1-B}{1+e^{\left(-\left(V-V_{½,b}\right)/s_b\right)}}+B\right)*\left(\frac{1-C}{1+e^{\left(-\left(V-V_{½,c}\right)/s_c\right)}}+C\right) \quad [2]$$

where the parameters $V_{½,b}$ and $V_{½,c}$ are half-maximal voltages, s_b and s_c are slopes, and B and C are the relative conductance at depolarized and hyperpolarized voltages, respectively. All curve fittings were performed using IGOR Pro software (Wavemetrics Inc.). In each figure, the data from individual experiments are shown while the summary data are reported as mean ± SEM (*SI Appendix*, Table S1).

Modeling the Allosteric Activation of spHCN Channels. GV relations for both wild-type and mutant spHCN channels were fit using a modular gating scheme adapted from a model developed by Horrigan and Aldrich for BK channels (HA model, Fig. 2) (35). In the HA model, the gating mechanism was viewed as a series of allosterically coupled conformational changes in different modules (domains) of the channel (Fig. 2*A*). This modular gating scheme assumes the PD has only one pore gate which is coupled to four VSDs and four CNBDs. Each domain was modeled as a reversible transition between two conformational states: the PD had a closed (C_{PD}) and open (O_{PD}) state, the VSD had a depolarized (R_{VSD}) and hyperpolarized (A_{VSD}) state, and the CNBD had a resting (R_{CNBD}) and activated (A_{CNBD}) state. The voltage-dependent equilibrium of the VSD between the R_{VSD} and A_{VSD} states was coupled to the voltage-independent equilibrium between C_{PD} and O_{PD} states of the PD such that opening was *F*-fold more favorable when each VSD was in the A_{VSD} state (and reciprocally each VSD equilibrium was *F*-fold more favorable when the PD was open). Similarly, the C_{PD} to O_{PD} transition was coupled to the activated state of each CNBD such that opening was *C*-fold more favorable when each CNBD was in the A_{CNBD} state (and reciprocally the CNBD activation was *C*-fold more favorable in the open state). Finally the HA model allowed for direct coupling between the VSD and CNBD modules (*E*).

The HA model was parameterized assuming that the allosteric coupling between the VSDs and the PD and between the CNBDs and PD were auto-inhibitory at rest (Fig. 2*A* and *SI Appendix*, S5). The equilibrium constant of the C_{PD} to O_{PD} transition of the PD at hyperpolarized voltages in the presence of cAMP was defined as *L*. The equilibrium constant of the R_{VSD} to A_{VSD} transition of the VSD with an open pore was defined as *H*. Finally, the equilibrium constant of the R_{CNBD} to A_{CNBD} transition of the CNBD was defined as *K*. In our HA model, the equilibrium constant *K* was not the bimolecular equilibrium constant for cyclic nucleotide binding. Instead, it was the equilibrium constant between the R_{CNBD} and A_{CNBD} states of the CNBD with bound cAMP or cGMP. The partial agonism of cGMP was reflected in the different *K* values for cAMP and cGMP which was shown previously using DEER spectroscopy on the isolated C-linker/CNBD of HCN channels (51). For an auto-inhibitory mechanism, the R_{VSD} state of the VSD caused the opening equilibrium constant to decrease to L/F^4, and the R_{CNBD} state of the CNBD caused the opening equilibrium constant to decrease to L/C^4. The VSD module was parameterized as auto-inhibitory because a large number of the mutations in this paper increased the conductance at depolarizing voltages without changing the apparent *L* at hyperpolarizing voltages. The HA models parameterized as auto-excitatory and auto-inhibitory are thermodynamically equivalent and predict identical values of *F*, so the changes in VSD-PD coupling predicted by the model do not depend on this parameterization. The steady-state open probability was calculated from the HA model using the following equation:

$$P_o=\frac{L/(C^4F^4)*(1+H/E+K/E+HK/E)^4}{L/(C^4F^4)*(1+H/E+K/E+HK/E)^4+(1+H/(FE)+K/(CE)+HK/(CEF))^4} \quad [3]$$

where the voltage-dependent equilibrium constant for the VSD was given by:

$$H(V)=H_0e^{(V/V_H)}. \quad [4]$$

Since there is no evidence to support coupling between the VSD and CNBD domains, the coupling factor between these two domains, *E*, was assumed to be 1. As a result, normalized conductance-voltage relationships were calculated from the HA model using the following equation:

$$\frac{G(V)}{Gmax,\, cAMP}=\frac{\alpha*L*(1/F+H/F)^4}{(1+H/F)^4+\alpha*L*(1/F+H/F)^4}*\left(\frac{1+L}{L}\right) \quad [5]$$

where

$$\alpha = \left(\frac{1+K}{C+K}\right)^4 \quad [6]$$

All the mutations in this investigation were made outside the CNBD domain and therefore the factors *K* and *C* were assumed to be unchanged by the mutations. In other words, the effect of the mutations were assumed to be on the energetics of modules outside the CNBD. Since the conformational changes outside the CNBD are thought to be structurally identical (although with different energetics) when either cAMP or cGMP are bound to the CNBD, the changes in fractional activation ($G_{cGMP}/G_{max,cAMP}$) by our mutations are assumed to arise from cyclic nucleotide-independent changes in the free energy of opening. This assumption has been verified for a large number of mutations and modification of CNG and HCN channels (4, 32, 33, 52, 53). Here, *L* was defined as the equilibrium constant for opening in the presence of saturating cAMP so *α_cAMP* was constrained to 1. The value for *α_cGMP* (0.091) was experimentally determined from previous noise analysis studies that determined the open probability of $spHCN_{WT}$ channels in saturating cAMP and cGMP at hyperpolarized voltages (32).

The fits of the HA model to the GV data were unique when the relative conductance at depolarized voltages was significant. One parameter that was not always well determined from the fitting was *F* for channels where the open probability at depolarizing voltages was low. Previously, Yellen and colleagues showed that cadmium block of spHCN-T464C channels in the presence of cAMP predicts an open probability of 6×10^{-4} at depolarized voltages (28). Therefore, for channels where the open probability at depolarized voltages was low, which includes $spHCN_{WT}$, the VSD-PD coupling factor was constrained to *F* equal to 10.1, which corresponds to an open probability of 6×10^{-4} at depolarized voltages.

Our threshold for being able to measure the coupling coefficient *F* was a steady-state conductance in cAMP at depolarized voltages that was more than 3% of the conductance at hyperpolarized voltages. This was more than two standard deviations larger than the relative conductance measured at depolarized voltages in $spHCN_{WT}$ (see *SI Appendix*, Table S1). At this threshold, *F* equal to 4 for the wild-type value of *L*. This calculation illustrates that *F* would have to be decreased more than two-fold to observe it. For this reason, small changes in *F* were not interpreted. The conclusions in this paper were based on mutations that produce large changes in *F* (e.g., spHCN-A4 or spHCN-E356A) or were expected to produce large changes in *F* but did not (e.g., $spHCN_{(359:363)}$).

The HA model was simultaneously fit to the GV curves at 1 mM cAMP and cGMP using a global fit function in IGOR Pro software (Wavemetrics Inc.). For most spHCN mutants, the GV fits had four free parameters: H_0 (the equilibrium constant for activation of the VSD at 0 mV with an open pore), V_H (the slope-factor that describes the voltage dependent rearrangement of the VSD), *L* (the equilibrium constant of pore opening with an activated VSD and cAMP-bound CNBD), and *F* (the coupling coefficient between the VSD and the PD). V_H is the voltage change that produced an e-fold change in

H and is defined by V_H = kT/z where k is Boltzmann's constant, T is temperature in °K, and z is the equivalent gating charge. For some mutants, the fitting parameters that were poorly determined were held constant as indicated in the text. The model occasionally predicted a small hyperpolarizing shift in the GV curve for cGMP and a lower fractional activation by cGMP at depolarized voltages. This limitation of the model could be largely alleviated by removing the constraint that *E* was equal to 1. Data were tabulated as mean ± SEM (Tables 1 and 2). Statistical comparisons were made using an online one-way ANOVA for summary data followed by a Tukey HSD post-hoc test at a confidence level of 95% (http://statpages.info/anova1sm.html). In addition, an online one-way *t* test was used to compare the difference of an observed mean with a constrained value for *F* of $spHCN_{WT}$ channels (https://www.medcalc.org/calc/test_one_mean.php).

ACKNOWLEDGMENTS. We thank Dr. John Bankston for his support and helpful discussions; Sharon Cunningham, Jane Simonsen, Finn Callahan, and Bailey Flynn, whose support helped this project stay on its successful trajectory; Megan Drews and Ximena Optiz-Araya for animal care and surgical support; and all members of the W.N.Z. laboratory for their support. This work was funded by NIH Grants R01MH102378 and R01EY010329 and American Heart Association Award 14CSA20380095 (to W.N.Z.), and by University of Washington Royal Research Award A56940 (to G.E.F.).

1. Robinson RB, Siegelbaum SA (2003) Hyperpolarization-activated cation currents: From molecules to physiological function. *Annu Rev Physiol* 65:453–480.
2. Biel M, Wahl-Schott C, Michalakis S, Zong X (2009) Hyperpolarization-activated cation channels: From genes to function. *Physiol Rev* 89:847–885.
3. Zagotta WN, Siegelbaum SA (1996) Structure and function of cyclic nucleotide-gated channels. *Annu Rev Neurosci* 19:235–263.
4. Craven KB, Zagotta WN (2006) CNG and HCN channels: Two peas, one pod. *Annu Rev Physiol* 68:375–401.
5. James ZM, Zagotta WN (2018) Structural insights into the mechanisms of CNBD channel function. *J Gen Physiol* 150:225–244.
6. Santoro B, Tibbs GR (1999) The HCN gene family: Molecular basis of the hyperpolarization-activated pacemaker channels. *Ann N Y Acad Sci* 868:741–764.
7. Santoro B, et al. (1998) Identification of a gene encoding a hyperpolarization-activated pacemaker channel of brain. *Cell* 93:717–729.
8. Ludwig A, Zong X, Jeglitsch M, Hofmann F, Biel M (1998) A family of hyperpolarization-activated mammalian cation channels. *Nature* 393:587–591.
9. Lee CH, MacKinnon R (2017) Structures of the human HCN1 hyperpolarization-activated channel. *Cell* 168:111–120.e11.
10. Long SB, Campbell EB, Mackinnon R (2005) Voltage sensor of Kv1.2: Structural basis of electromechanical coupling. *Science* 309:903–908.
11. Long SB, Campbell EB, Mackinnon R (2005) Crystal structure of a mammalian voltage-dependent Shaker family K+ channel. *Science* 309:897–903.
12. Wang W, MacKinnon R (2017) Cryo-EM structure of the open human ether-à-go-go-related K^+ channel hERG. *Cell* 169:422–430.e10.
13. Tao X, Hite RK, MacKinnon R (2017) Cryo-EM structure of the open high-conductance Ca^{2+}-activated K^+ channel. *Nature* 541:46–51.
14. Sun J, MacKinnon R (2017) Cryo-EM structure of a KCNQ1/CaM complex reveals insights into congenital long QT Syndrome. *Cell* 169:1042–1050.e9.
15. James ZM, et al. (2017) CryoEM structure of a prokaryotic cyclic nucleotide-gated ion channel. *Proc Natl Acad Sci USA* 114:4430–4435.
16. Li M, et al. (2017) Structure of a eukaryotic cyclic-nucleotide-gated channel. *Nature* 542:60–65.
17. Vemana S, Pandey S, Larsson HP (2004) S4 movement in a mammalian HCN channel. *J Gen Physiol* 123:21–32.
18. Männikkö R, Elinder F, Larsson HP (2002) Voltage-sensing mechanism is conserved among ion channels gated by opposite voltages. *Nature* 419:837–841.
19. Bell DC, Yao H, Saenger RC, Riley JH, Siegelbaum SA (2004) Changes in local S4 environment provide a voltage-sensing mechanism for mammalian hyperpolarization-activated HCN channels. *J Gen Physiol* 123:5–19.
20. Lu Z, Klem AM, Ramu Y (2002) Coupling between voltage sensors and activation gate in voltage-gated K+ channels. *J Gen Physiol* 120:663–676.
21. Lu Z, Klem AM, Ramu Y (2001) Ion conduction pore is conserved among potassium channels. *Nature* 413:809–813.
22. Fernández-Mariño AI, Harpole TJ, Oelstrom K, Delemotte L, Chanda B (2018) Gating interaction maps reveal a noncanonical electromechanical coupling mode in the Shaker K^+ channel. *Nat Struct Mol Biol* 25:320–326.
23. Blunck R, Batulan Z (2012) Mechanism of electromechanical coupling in voltage-gated potassium channels. *Front Pharmacol* 3:166.
24. Kalstrup T, Blunck R (2018) S4–S5 linker movement during activation and inactivation in voltage-gated K^+ channels. *Proc Natl Acad Sci USA* 115:E6751–E6759.
25. Prole DL, Yellen G (2006) Reversal of HCN channel voltage dependence via bridging of the S4-S5 linker and post-S6. *J Gen Physiol* 128:273–282.
26. Rothberg BS, Shin KS, Phale PS, Yellen G (2002) Voltage-controlled gating at the intracellular entrance to a hyperpolarization-activated cation channel. *J Gen Physiol* 119:83–91.
27. Gauss R, Seifert R, Kaupp UB (1998) Molecular identification of a hyperpolarization-activated channel in sea urchin sperm. *Nature* 393:583–587.
28. Kwan DC, Prole DL, Yellen G (2012) Structural changes during HCN channel gating defined by high affinity metal bridges. *J Gen Physiol* 140:279–291.
29. Decher N, Chen J, Sanguinetti MC (2004) Voltage-dependent gating of hyperpolarization-activated, cyclic nucleotide-gated pacemaker channels: Molecular coupling between the S4-S5 and C-linkers. *J Biol Chem* 279:13859–13865.
30. Guex N, Peitsch MC (1997) SWISS-MODEL and the Swiss-PdbViewer: An environment for comparative protein modeling. *Electrophoresis* 18:2714–2723.
31. Shin KS, Rothberg BS, Yellen G (2001) Blocker state dependence and trapping in hyperpolarization-activated cation channels: Evidence for an intracellular activation gate. *J Gen Physiol* 117:91–101.
32. Flynn GE, Black KD, Islas LD, Sankaran B, Zagotta WN (2007) Structure and rearrangements in the carboxy-terminal region of SpIH channels. *Structure* 15:671–682.
33. Flynn GE, Zagotta WN (2011) Molecular mechanism underlying phosphatidylinositol 4,5-bisphosphate-induced inhibition of SpIH channels. *J Biol Chem* 286:15535–15542.
34. Wainger BJ, DeGennaro M, Santoro B, Siegelbaum SA, Tibbs GR (2001) Molecular mechanism of cAMP modulation of HCN pacemaker channels. *Nature* 411:805–810.
35. Horrigan FT, Aldrich RW (2002) Coupling between voltage sensor activation, Ca2+ binding and channel opening in large conductance (BK) potassium channels. *J Gen Physiol* 120:267–305.
36. Shin KS, Maertens C, Proenza C, Rothberg BS, Yellen G (2004) Inactivation in HCN channels results from reclosure of the activation gate: Desensitization to voltage. *Neuron* 41:737–744.
37. Lörinczi É, et al. (2015) Voltage-dependent gating of KCNH potassium channels lacking a covalent link between voltage-sensing and pore domains. *Nat Commun* 6:6672.
38. Biel M, Michalakis S (2009) Cyclic nucleotide-gated channels. *Handb Exp Pharmacol,* 111–136.
39. Mazzolini M, Marchesi A, Giorgetti A, Torre V (2010) Gating in CNGA1 channels. *Pflugers Arch* 459:547–555.
40. Ryu S, Yellen G (2012) Charge movement in gating-locked HCN channels reveals weak coupling of voltage sensors and gate. *J Gen Physiol* 140:469–479.
41. de la Peña P, Domínguez P, Barros F (2018) Gating mechanism of Kv11.1 (hERG) K^+ channels without covalent connection between voltage sensor and pore domains. *Pflugers Arch* 470:517–536.
42. Tomczak AP, et al. (2017) A new mechanism of voltage-dependent gating exposed by K_V10.1 channels interrupted between voltage sensor and pore. *J Gen Physiol* 149:577–593.
43. del Camino D, Yellen G (2001) Tight steric closure at the intracellular activation gate of a voltage-gated K(+) channel. *Neuron* 32:649–656.
44. del Camino D, Holmgren M, Liu Y, Yellen G (2000) Blocker protection in the pore of a voltage-gated K+ channel and its structural implications. *Nature* 403:321–325.
45. Larsson HP, Baker OS, Dhillon DS, Isacoff EY (1996) Transmembrane movement of the shaker K+ channel S4. *Neuron* 16:387–397.
46. Whicher JR, MacKinnon R (2016) Structure of the voltage-gated K^+ channel Eag1 reveals an alternative voltage sensing mechanism. *Science* 353:664–669.
47. Yifrach O, MacKinnon R (2002) Energetics of pore opening in a voltage-gated K(+) channel. *Cell* 111:231–239.
48. Islas LD, Sigworth FJ (1999) Voltage sensitivity and gating charge in Shaker and Shab family potassium channels. *J Gen Physiol* 114:723–742.
49. Liman ER, Tytgat J, Hess P (1992) Subunit stoichiometry of a mammalian K+ channel determined by construction of multimeric cDNAs. *Neuron* 9:861–871.
50. Hamill OP, Marty A, Neher E, Sakmann B, Sigworth FJ (1981) Improved patch-clamp techniques for high-resolution current recording from cells and cell-free membrane patches. *Pflugers Arch* 391:85–100.
51. DeBerg HA, Brzovic PS, Flynn GE, Zagotta WN, Stoll S (2016) Structure and Energetics of Allosteric Regulation of HCN2 Ion Channels by Cyclic Nucleotides. *J Biol Chem* 291:371–381.
52. Gordon SE, Zagotta WN (1995) A histidine residue associated with the gate of the cyclic nucleotide-activated channels in rod photoreceptors. *Neuron* 14:177–183.
53. Craven KB, Zagotta WN (2004) Salt bridges and gating in the COOH-terminal region of HCN2 and CNGA1 channels. *J Gen Physiol* 124:663–677.